



NOISE-CON 94

Ft. Lauderdale, Florida

1994 May 01-04

SOUND RADIATION FROM STRUCTURES IN THE PRESENCE OF CLOSE-FITTING SOUND SHIELDS

F. Augustinovicz, P. Sas and F. Penne

**Katholieke Universiteit Leuven
Mechanical Engineering Department
Celestijnenlaan 300B, B-3001 Leuven, Belgium**

Introduction

The noise emitted by machines or vehicle engines is often reduced by using close-fitting enclosures which, due to technical constraints, most frequently can only be implemented in the form of a partial enclosure or as a simple sound shield only. The acoustical performance of these elements depends on a great variety of physical mechanisms and parameters and, consequently, is difficult to predict [1]. One of these parameters is the back reaction of the shield on the radiating characteristics of the source.

The effect is well known and exhaustively discussed for some elementary sources in the literature of theoretical acoustics [2-5]. The radiation from a rectangular panel into a shallow, infinite cavity was investigated both theoretically and experimentally by Schroter and Fahy [6] and by Verheij [7]. Nevertheless, the increased radiation load of the sources, caused by the presence of the shield is usually not considered in the literature of acoustic enclosures [8,9] or only shortly mentioned without detailed treatment [10]. A very recent analysis, dealing with a closely related problem by theoretical and numerical means, is to be published soon by Verheij et al. [11]

The aim of this paper is to investigate how the radiated power from a simple test structure is influenced by the presence of a rigid, plane shield. The new aspect of our investigation is that the overall radiation from a free-standing three-dimensional structure, shielded with a relatively small reflector is considered by using an experimental approach. Note that a simultaneous, extended numerical investigation of the subject is in progress. The results of the numerical counterpart of the work reported herein can be found elsewhere [12,13] and, due to size constraints, only some references to the results of the numerical calculations can be made here.

Theoretical considerations and measuring methods

The power radiated from a vibrating structure can be calculated by integrat-

ing the acoustic intensity I over a closed surface A :

$$P = \oint_A I_n dA = \frac{I}{2} \oint_A \text{Re} \{ p u_n^* \} dA = \frac{I}{2} \oint_A |p| |u_n| \cos(\varphi_p - \varphi_{u_n}) dA \quad (1)$$

where the index n means the vector components normal to the surface element dA . Due to the continuity relation the particle velocity u on the surface of the radiator (further denoted as S) is equal to the surface velocity v of the structure. Introducing an impedance Z_F , defined on S as

$$Z_F = \frac{p}{v_n} = \frac{|p|}{|v_n|} \left(\cos(\varphi_p - \varphi_{v_n}) + j \sin(\varphi_p - \varphi_{v_n}) \right) \quad (2)$$

the power radiated to the far-field can be calculated by the integrals

$$P = \frac{I}{2} \oint_S R_F |v_n|^2 dS = \frac{I}{2} R \oint_S |v_n|^2 dS \quad (3)$$

where R_F , the real part of the specific impedance Z_F (denoted as field impedance after Mechel [14]) is obviously a space dependent quantity along the surface of the radiator and R is the usual, overall radiation resistance.

Comparing Eqs. (1) and (2) the close relationship between the intensity and the field impedance is obvious. The field impedance is directly obtainable for any point of the radiator's surface by using a sensor pair consisting of an accelerometer and a microphone, just like in case of surface intensity measurements [15].

Following the analogy, the accuracy of the field impedance measurement highly depends on the phase characteristics of the measurement channels, too [16]. The phase mismatch between the used microphones (miniature electret microphones of type AKG CK 67-3) and accelerometers (PCB 303A) was checked by using a converted acoustic impedance tube of B&K 4002 as shown in Fig. 1. A rigid aluminium disc, supported and sealed by a rubber plate at one end of the tube was assumed to generate plane waves in the tube. The tube was filled with glasswool in the way as shown in the figure, to realize anechoic termination of the other end. The field impedance was measured in the central part of the disc for 8 sensor pairs; a typical calibration impedance curve is shown in Fig. 2. Since the phase error was not too high, no phase correction was used [17]. One has nevertheless to be aware that those parts of the impedance curves, where the pressure and the velocity is appr. 90° out of phase, are unreliable.

Test set-up

The investigations were based on a simple steel structure, shaped such as to bear some resemblance to an engine block. Although smaller in size, it was designed to have similar natural frequencies to those of a real-life diesel engine, thus resulting in some sort of a scale model or engine mock-up. In the present phase of the investigations the frequency range of the measurements was restricted to below 1 kHz, in order to be in harmony with the requirements of the numerical calculations. A welded steel box of dimensions 400*300*150 mm with plate thickness of

5 mm was fabricated with a bulkhead inside, and closed at the bottom with a PVC plate which was resiliently connected to the box. The development of the mock-up was completed by performing an EMA test. Some typical mode shapes of the structure are shown in Fig. 3; more details about the structure can be found in [12].

The structure was then placed on a pedestal in a semi-anechoic room. An electrodynamic shaker was used to exert a point force on one side of the structure while the shield (a rigid, structurally damped steel plate of 3 mm thickness) was placed on the other side, parallel to the structure at a distance of 50 mm. The normal component of the sound intensity was measured along a field point mesh, consisting of three rectangular measurement planes normal to each other and located at 150 mm distance (See Fig. 4) from the source. The pressures and surface accelerations were measured in 8 points as marked on Fig.3. in terms of FRF's, referenced to the input force, then processed to obtain the field impedance as defined in Eq.(2). All measurements were performed both under free-field conditions and with the sound shield in place.

Measurement results

Fig. 5a. shows the intensity spectra, measured and summed along all three field point surfaces, and the obtained overall insertion loss (further referred to as IL) is shown in Fig. 5b. Since the radiating structure is lightly damped, the intensity functions show distinct peaks while the IL curve is rather smooth. It is striking, that the presence of the shield increases rather than reduces the overall radiated power for almost all frequencies.

A more detailed insight can be gained by calculating and depicting the spatial variation of the IL for some selected frequencies or frequency bands. As an example, the contour plot of the IL for 533 Hz (the frequency of the highest radiation peak) is shown in Fig.6. As one can anticipate for a complex radiator, surrounded by a shield of dimensions comparable with the wavelength in air, a complex interference field is brought about. Generally speaking, there is amplification rather than reduction behind the shield, the extent of which ranges from appr. zero in the middle of the measurement plane to some 15 dB around the edges. There is no significant level change along the side plane, but strongly varying insertion loss (with spots of slight level decreases but also increases up to 18 dB) can be observed on top of the box. The spatial variation of the shield performance is even more pronounced for higher frequencies and is slightly reduced when third-octave averaging is applied.

Another way of looking upon the modifying effect of the shield is to perform the spatial averaging separately for all three measurement planes. The intensity spectra, measured with and without shield and averaged for the measurement plane behind the shield are compared in Fig. 7a. while the IL is shown in Fig. 7b. The measured IL is verified by a calculated IL curve, derived from boundary element calculations [13] and depicted as a dotted line in Fig. 7b. as well. Fig. 7c. in turn depicts the spatially averaged contribution of the three measurement planes against frequency. By comparing the three curves one can draw the conclusion that the shield modifies the power flow from the structure mainly toward the top of the

structure, although considerable amount of sound energy is leaving the system behind the shield, too. On the other hand, the shield not only redirects but also increases the radiated power in absolute terms.

In order to determine, whether or not this increase may be entirely attributed to the increased radiation load of the structure, the acceleration and the sound pressure measured on or close to the surface, and the real part and phase angle of the field impedance is shown for two typical points in Fig. 8. and 9. Virtually no difference can be found in the surface vibration with and without shield, while the magnitude of the pressure is clearly influenced. However, the unchanged surface velocity does not imply that the radiation from the structure is unaffected as well. In point 7 (selected on the surface where high vibration amplitudes can be observed) the field resistance is positive and remains well below $420 \text{ kg/m}^2\text{s}$ without the shield (see Fig. 8c). The shield in turn considerably increases the field resistance (except for the resonance frequency at 660 Hz), thus giving rise to increased overall power radiation. In point 2 (located close to the bottom edge) the structure without the shield behaves as a local sink, characterised by a small negative resistance (see Fig. 9c). The shield seems to turn this sink into a source for frequencies between the radiation peaks. The "strength" of the sink is increased for the resonant frequency at 610 Hz but reduced for 660 Hz. All these observations are in good agreement with the overall insertion loss values as depicted in Fig. 5b.

Conclusions

The power, radiated from a simple mechanical structure can be significantly modified by the presence of a simple, undamped sound shield, even if the shield is applied on one side of the structure only. In the case of the investigated source-shield system the power was increased rather than reduced for most of the considered frequencies. The increase can be sufficiently explained by the increased radiation load of the shield. The surface vibration is not affected by the acoustic environment, therefore the use of an uncoupled numerical approach is fully justified.

Acknowledgement

The work reported herein was related to the EU Brite/Euram Research Project PIANO (under contract BRE2-0210). The project is supported by the Directorate-General for Science, Research and Development of the CEU.

References

1. Y.C.C. Sung and N. Lalor, Proc. IME Int. Conf., Birmingham, Paper C29/88 (1988)
2. U. Ingard and G.L. Lamb, *J. Acoust. Soc. Am.*, **29**, 743-744 (1957)
3. R. Waterhouse, *J. Acoust. Soc. Am.*, **30**, 4-13 (1958)
4. R. Waterhouse, *J. Acoust. Soc. Am.*, **35**, 1144-1151 (1963)
5. G.C. Maling, *J. Acoust. Soc. Am.*, **42**, 859-865 (1967)
6. V. Schroter and F.J. Fahy, *J. Sound Vib.*, **74**, 575-587 (1981)
7. J.W. Verheij, Ph.D. Thesis, Delft, 73-104.p. (1982)
8. L.W. Tweed and D.R. Tree, *Noise Control Eng.*, **10**, 74-79 (1978)

9. M.J.Crocker (Ed.), *Reduction of machinery noise*, 349-364 (Purdue U., W. Lafayette, 1975)
10. L.L. Beranek and I.L. Vér, *Noise and Vibration Control Engineering*, J. Wiley (1992), Ch.13.
11. J.W. Verheij et al, Paper submitted for the 3rd Int. Congr. Sound and Vib., Montreal (1994)
12. F. Augustinovicz and P. Sas, *Proc. Inter-Noise 93*, 721-726 (1993)
13. F. A., P. Sas and F. Penne, Paper submitted for Int. Sem. on Modal Analysis, Leuven (1994)
14. F.P. Mechel, *J. Sound Vib.*, **123**, 537-572 (1988)
15. N. Kaemmer and M.J. Crocker, *Proc. Noise-Con 79*, 153-160 (1979)
16. M.C. McGary and M.J. Crocker, *J. Sound Vib.*, **82**, 275-288 (1982)
17. K.B.Ginn, *Proc. Inter-Noise 84*, 1083-1086 (1984)

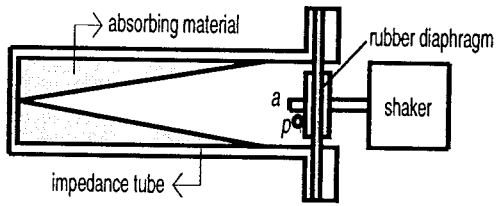


Figure 1 : Calibration set-up

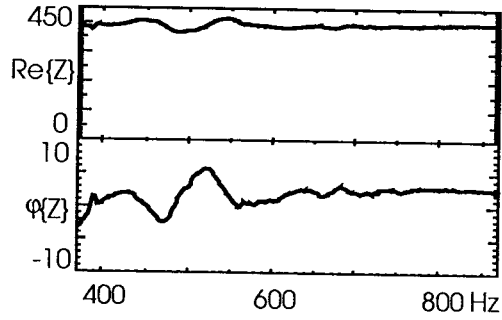


Figure 2 : Calibration curve

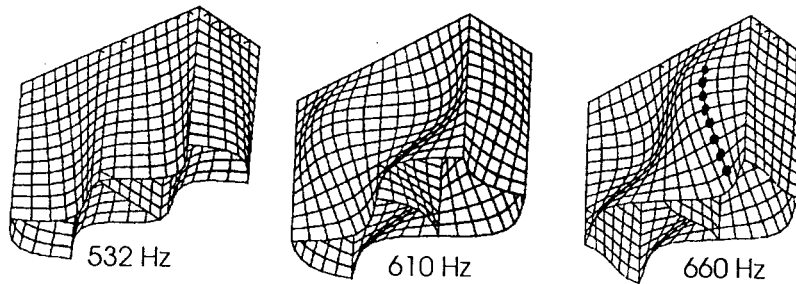


Figure 3 : Some important modeshapes

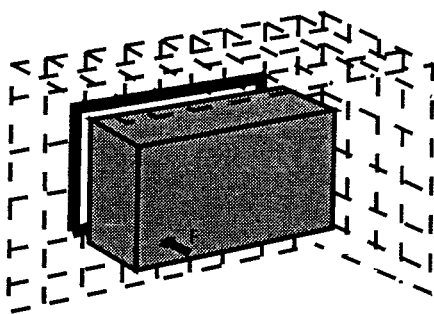


Figure 4 : Test structure with shield and field point mesh

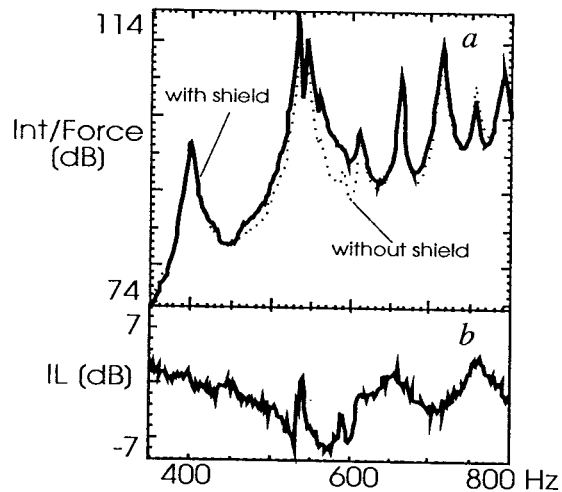


Figure 5 : Overall effect of the shield

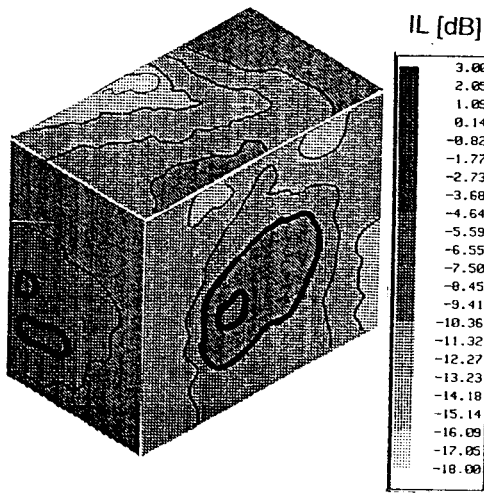


Figure 6 : Spatial variation of IL based on normal intensities

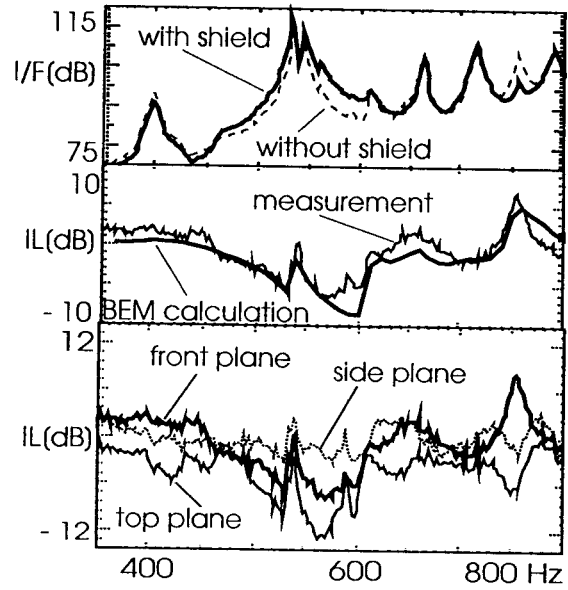


Figure 7 : Effect of the shield for various measurement planes (see text)

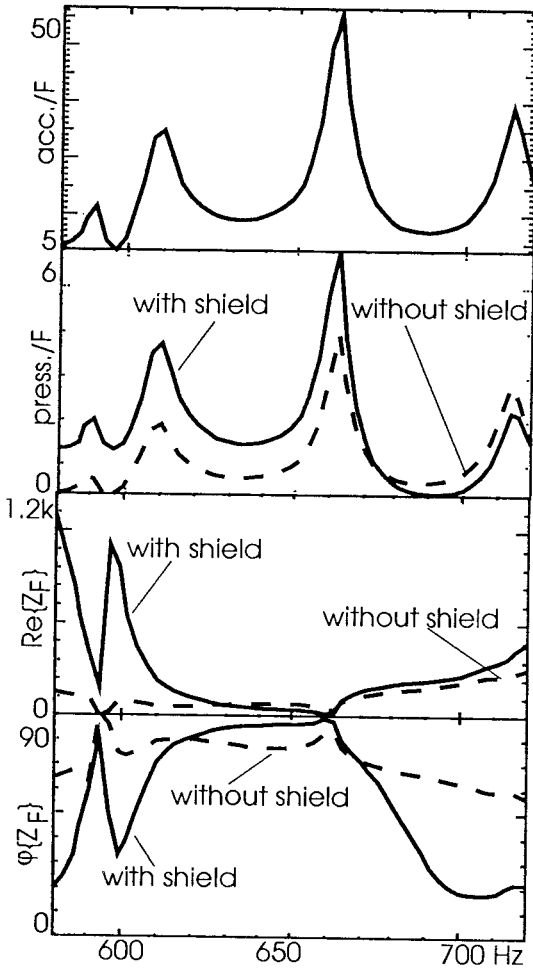


Figure 8 : Effect of shield for point 7

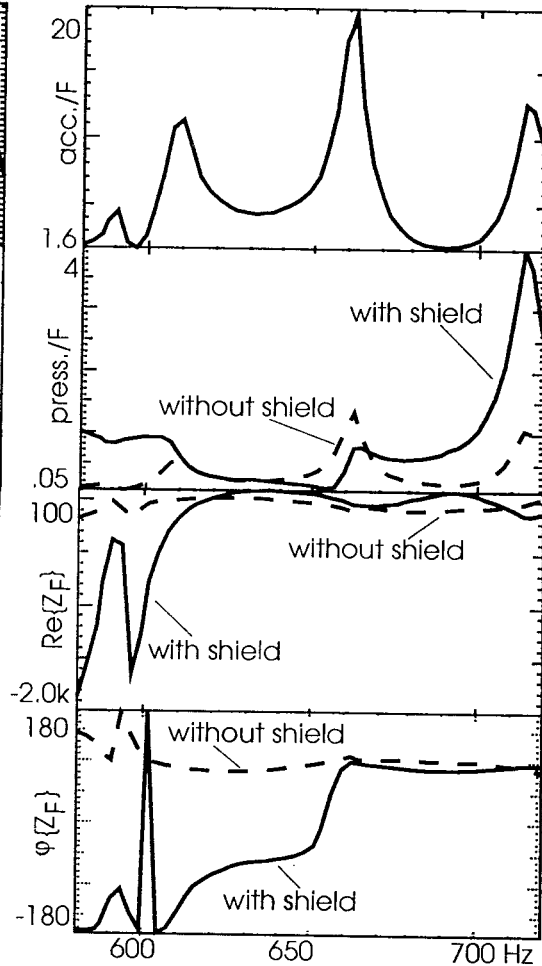


Figure 9 : Effect of shield for point 2